Electronic Supplementary Information

Construction of a series of Ln-MOFs Luminescent sensors based a functional "V" shaped ligand

*Xueguang Liu[a]†, Wei Liu[*b]†, Xiaoshan Yang[a], Yao Kou[a], Wanmin Chen[a], Weisheng Liu[*a]*

[a]Key Laboratory of Nonferrous Metal Chemistry and Resources Utilization of Gansu Province and State Key Laboratory of Applied Organic Chemistry, Key Laboratory of Special unction Materials and Structure Design, Ministry of Education, College of Chemistry and Chemical Engineering, Lanzhou University, Lanzhou 730000, China. Lanzhou 730000 (P.R. China). *E-mail: liuws@lzu.edu.cn.

[b]Institute of National Nuclear Industry, Frontiers Science Center for Rare Isotope, School of Nuclear Science and Technology, Key Laboratory of Special Function Materials and Structure Design, Ministry of Education, Lanzhou University, 730000, Lanzhou, China.

†These authors contributed equally to this work.

* Corresponding authors:
E-mail for Weisheng Liu: liuws@lzu.edu.cn
* Corresponding authors:
E-mail for Wei Liu: l_w@lzu.edu.cn

Materials and Instrumentation: All solvents and reagents were commercially available A.R. grade and used without further purification unless otherwise noted. Preparation of stock solutions: All the analytic solutions (Aniline, OPD, MPD, PPD) were prepared by separately dissolving each of them in DMF with a concentration of 0.1 M and 0.01M. Luminescence spectra were measured using a Hitachi F-7000 luminescence spectrometer. Fluorescent quantum yield was determined by an absolute method using an integrating sphere on FLS920 of Edinburgh Instrument. UV-visible spectra were recorded using an Agilent Cary 5000 spectrophotometer. The FT-IR spectra were recorded from KBr pellets in the range from 4000 to 500 cm^{-1} on a Bruker VERTEX 70 spectrometer. Powder X-Ray diffraction (PXRD) patterns were collected with a PAN alytical X'Pert Pro Diffractometer operated at 40 kV and 40 mA with Cu Kα radiation. Thermogravimetric analyses (TGA) were obtained on a NETZSCH STA 449 F3 Jupiter® under a N_2 atmosphere. ICP-MS (Agilent 7800).

X-ray Structural Crystallography: The single-crystal X-ray diffraction data of $C_{29}H_{35}EuN_4O_{13}$ was collected on SuperNova, Dual, Cu at zero, AtlasS2. The crystal was kept at 150(10) K during data collection. Using Olex2 [1], the structure was solved with the SHELXT [2] structure solution program using Intrinsic Phasing and refined with the SHELXL [3] refinement package using Least Squares minimisation.

1. Dolomanov, O.V., Bourhis, L.J., Gildea, R.J, Howard, J.A.K. & Puschmann, H. (2009), J. Appl. Cryst. 42, 339-341.
2. Sheldrick, G.M. (2015). Acta Cryst. A71, 3-8.
3. Sheldrick, G.M. (2015). Acta Cryst. C71, 3-8.

Calculations of Luminescent Quantum Yield: Luminescent quantum yield data was measured in the solid state at 298K, and the emission was monitored from 400 to 720 nm. The overall luminescent quantum yields of the solid-state samples were determined by an absolute method using an integrating sphere on FLS920 of Edinburgh Instrument (150 mm diameter, $BaSO_4$ coating) and acquired using the following equation:

$$\Phi_{overall} = (A_H) / (R_{ST} - R_H) \quad (S1)$$

where A_H is the area under emission spectrum of the sample and R_{ST} and R_H are diffuse reflectance of the reflecting standard and the sample, respectively.

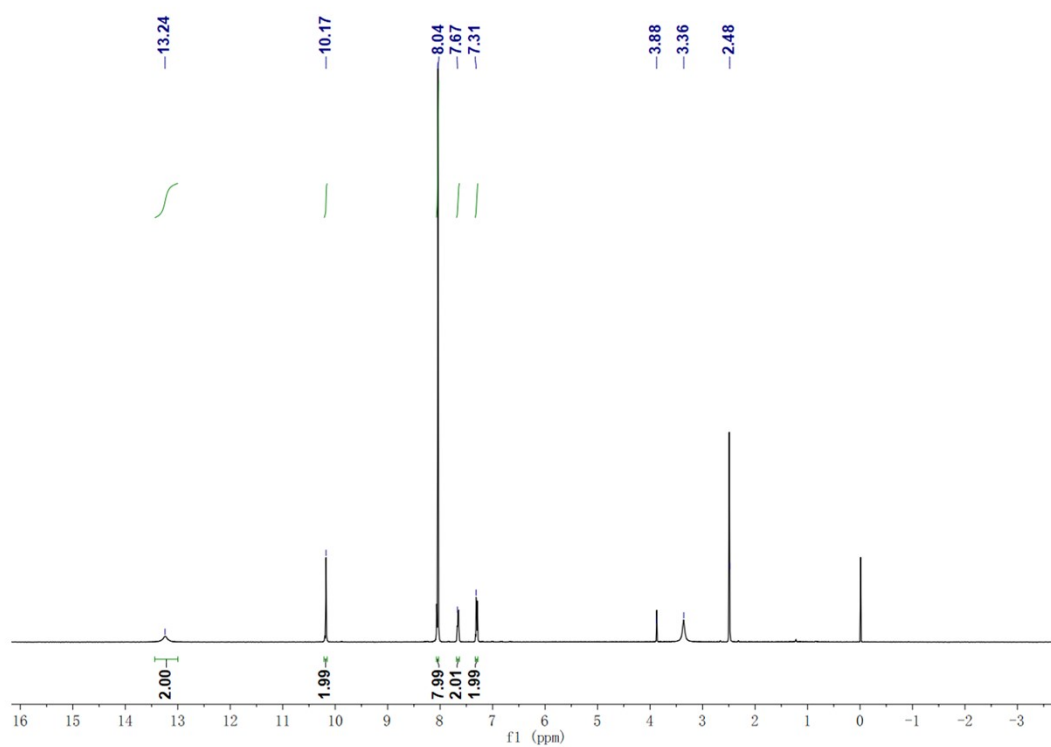# Additional Figures and Schemes:
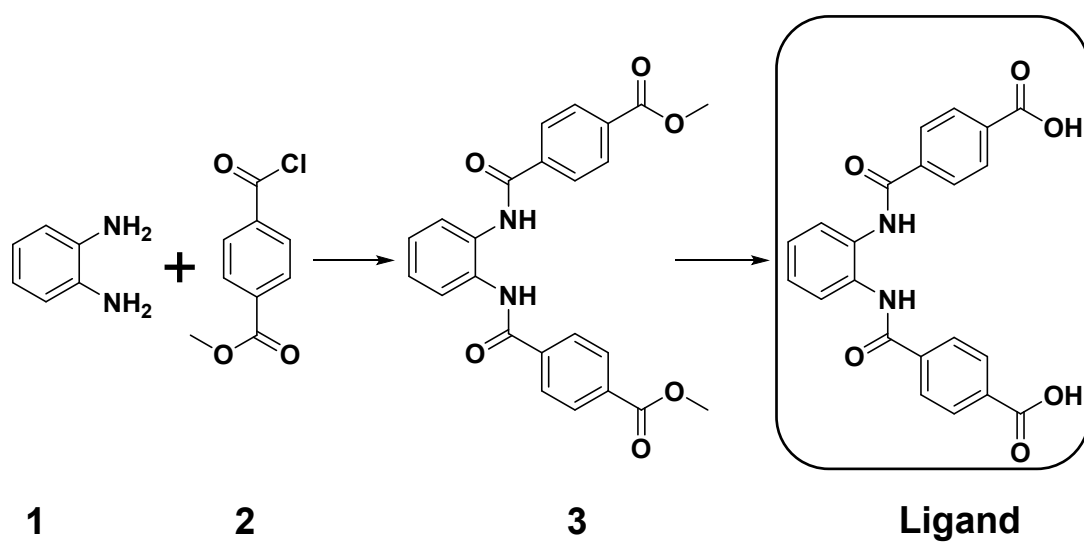
Scheme S1. Synthesis of Ligand.
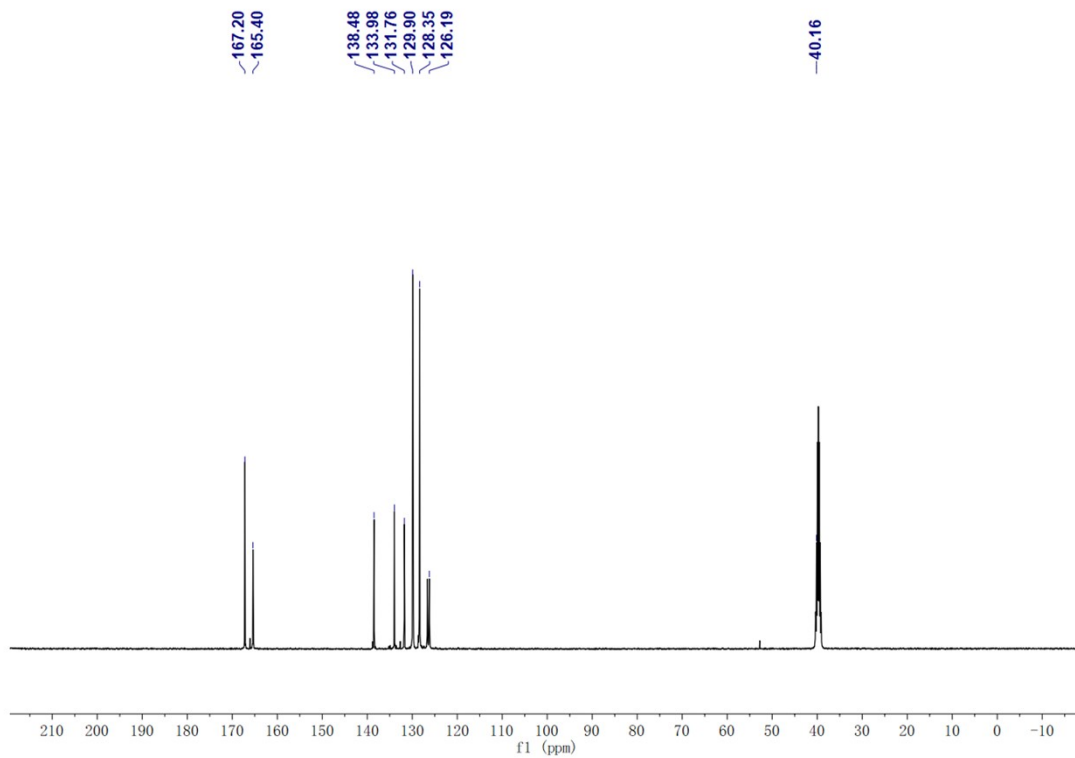

Figure S1. H NMR spectra of H_2L recorded in DMSO.

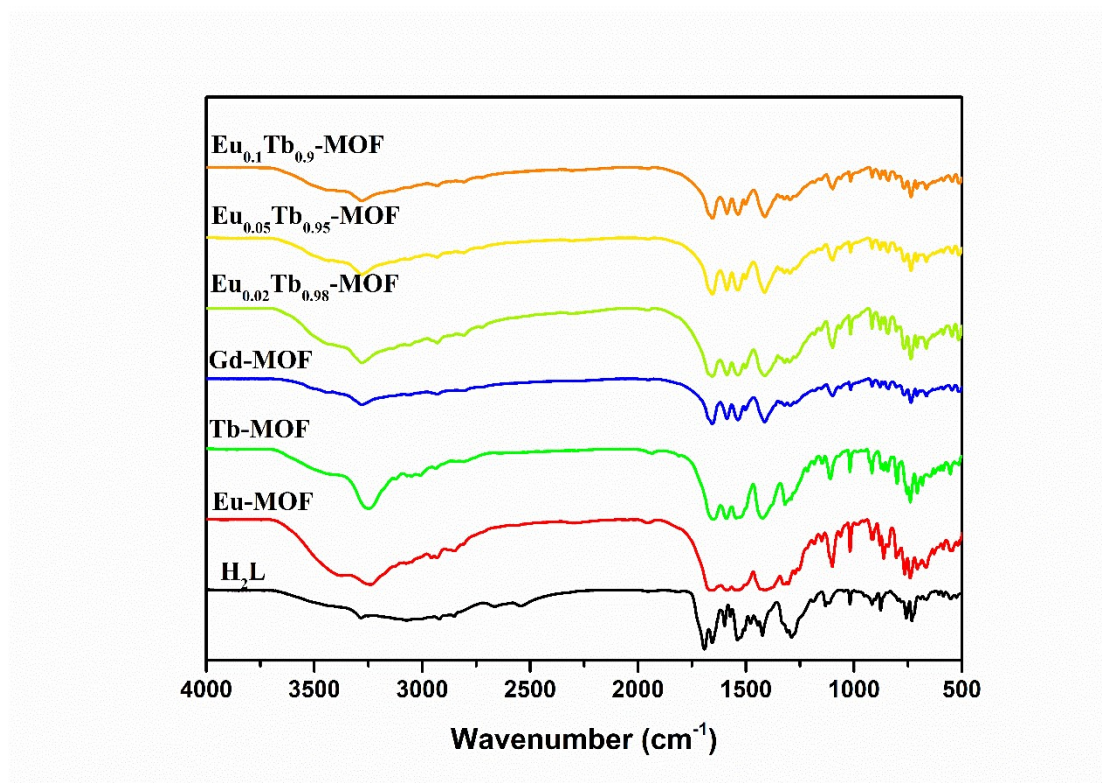**Figure S2.** ^{13}C NMR spectra of H_2L recorded in DMSO.

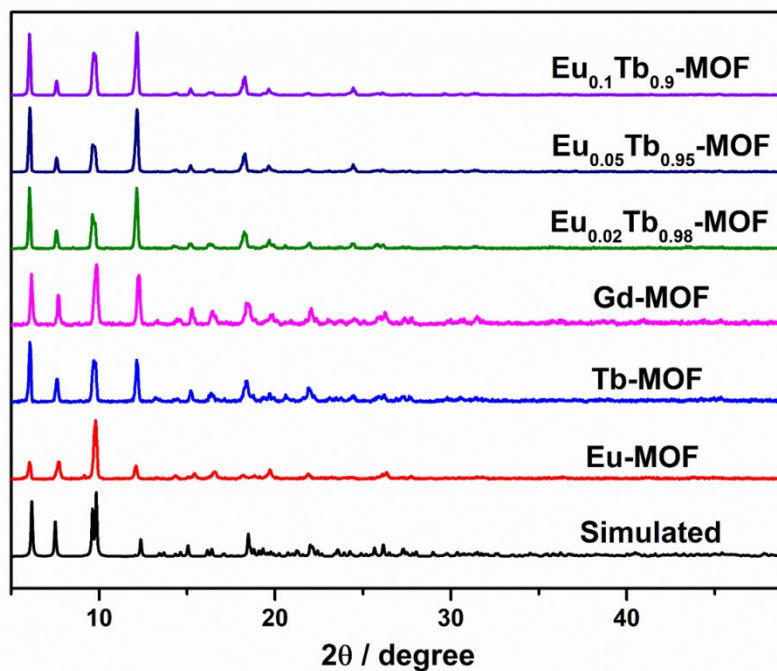**Fig S3.** IR spectra of H_2L and the Ln-MOFs.
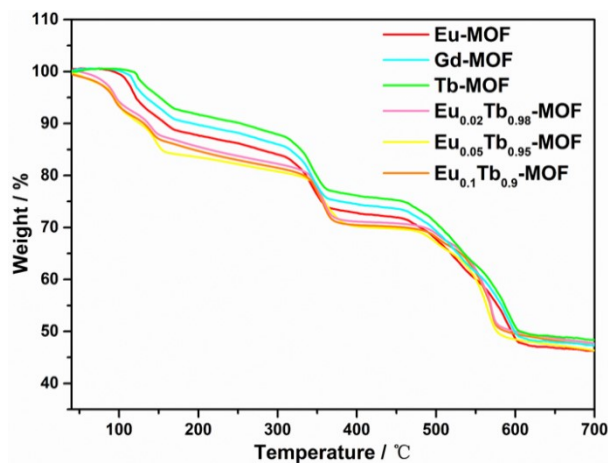
Fig S4. The PXRD of the synthesized Ln-MOFs.

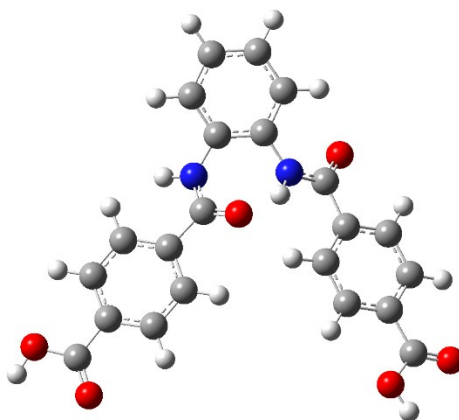
Fig S5. TGA plot of the Ln-MOFs

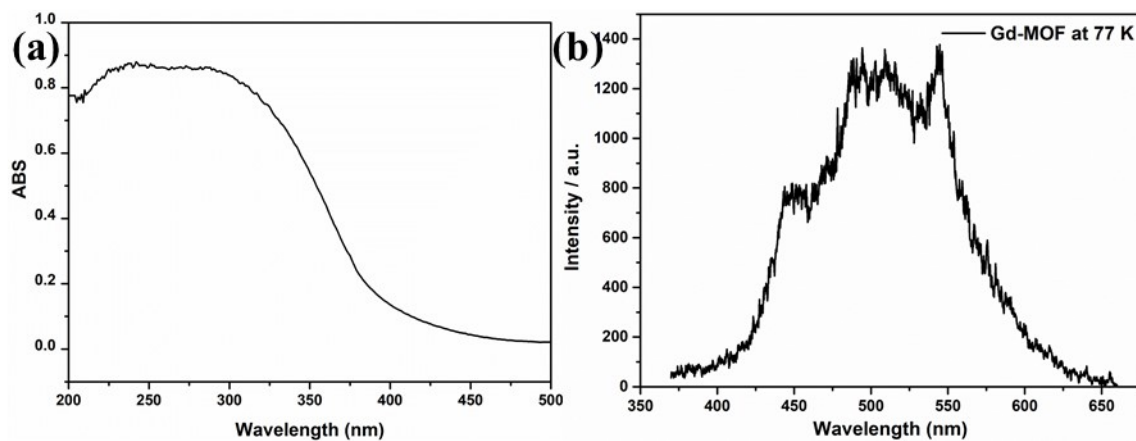**Fig S6.** The optimized geometry of the free H_2L

Fig S7. (a) UV-Vis absorption spectrum of H_2L; (b) Phosphorescence spectrum of the Gd-MOF at 77 K.
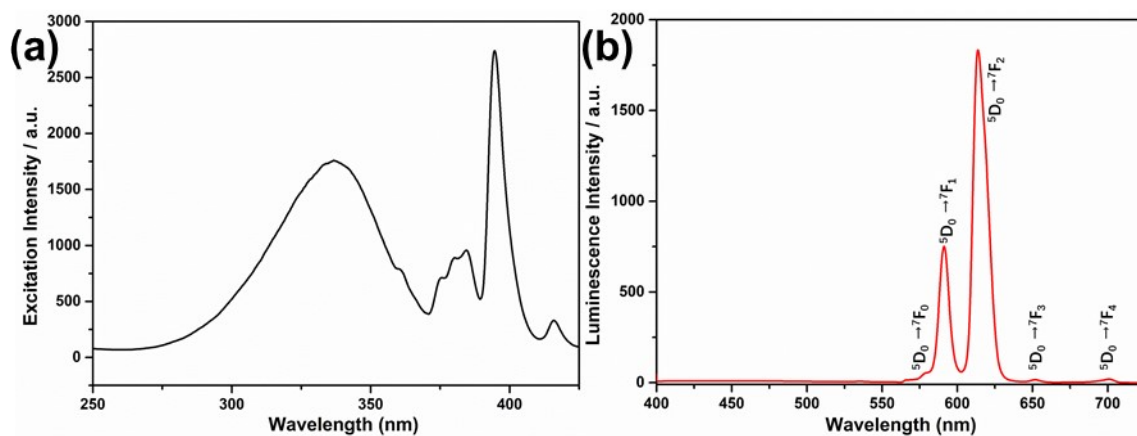

Fig S8. (a) The excited spectra of the Eu-MOF (λ_{em} = 614 nm); (b) The luminescence spectra of the Eu-MOF (λ_{em} = 340 nm).
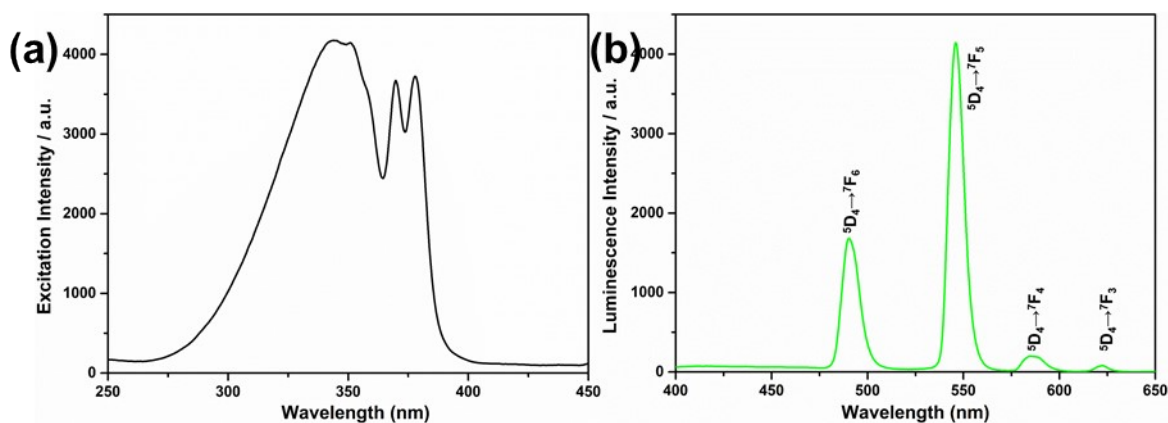

Fig S9. (a) The excited spectra of the Tb-MOF (λ_{em} = 546 nm); (b) The luminescence spectra of the Tb-MOF (λ_{em} = 340 nm).
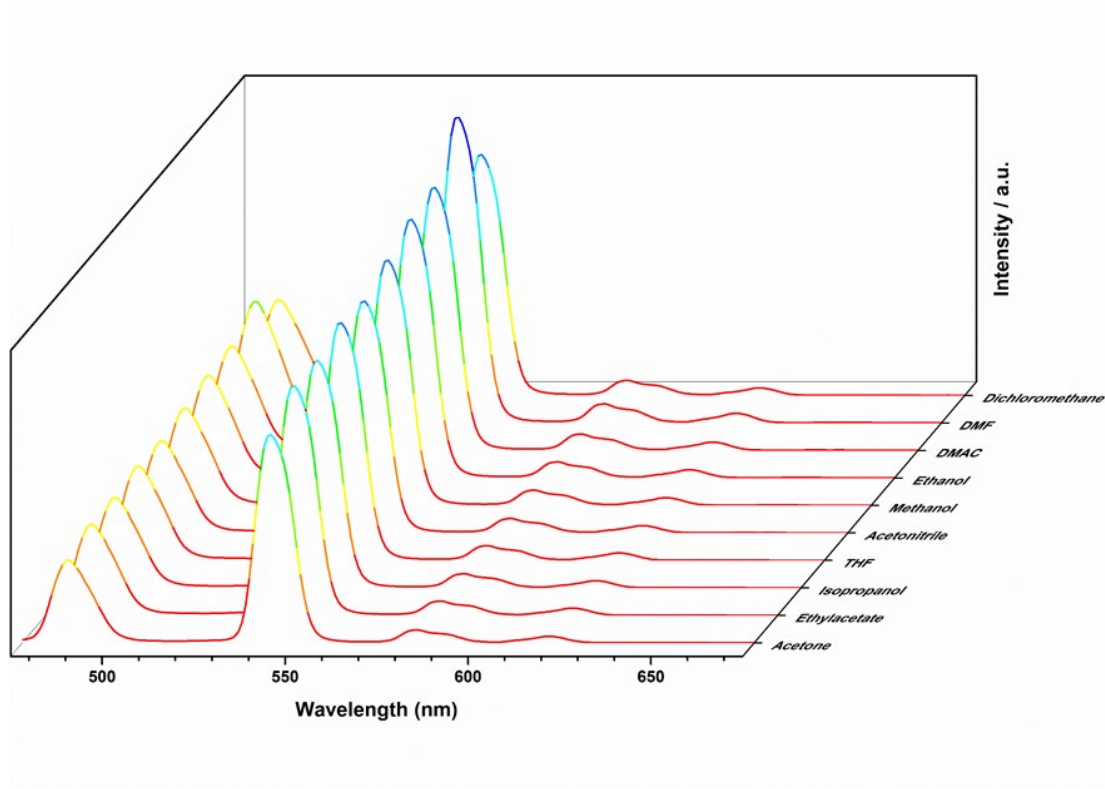
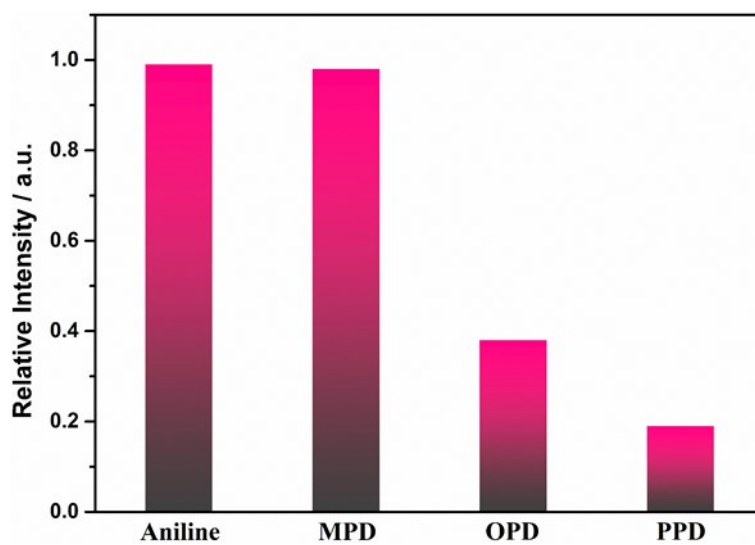**Fig S10.** Luminescence Spectra of the Tb-MOF in different organic solvents.

Fig S11. Luminescence change of the Eu-MOF after adding 1.5 mM amine.

Fig S12. (a) Luminescence spectra of the Eu-MOF in DMF when the concentration of PPD ranged from 0 to 1.5 mM; (b) The line were fitted by S-V equation.
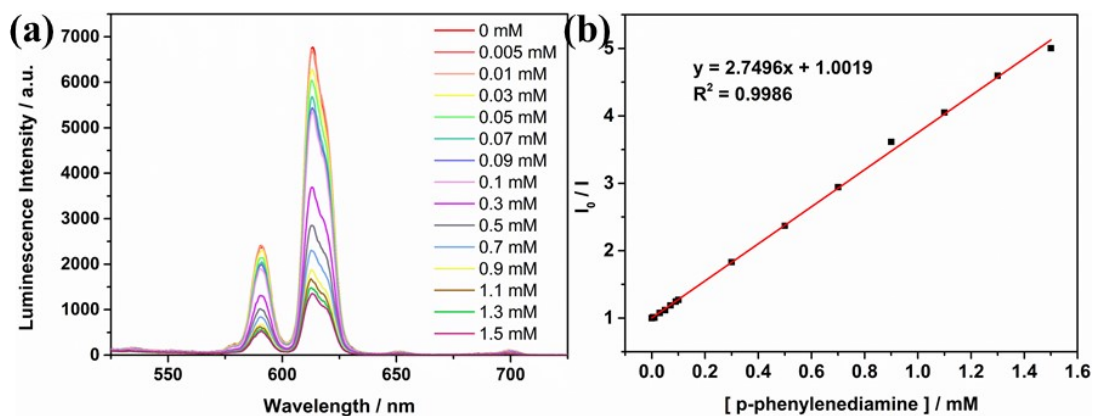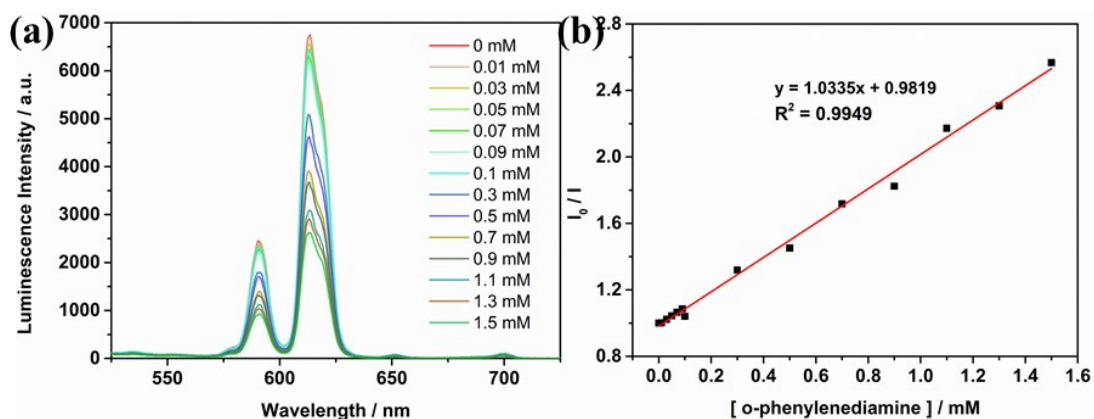

Fig S13. (a) Luminescence spectra of the Eu-MOF in DMF when the concentration of OPD ranged from 0 to 1.5 mM; (b) The line were fitted by S-V equation.
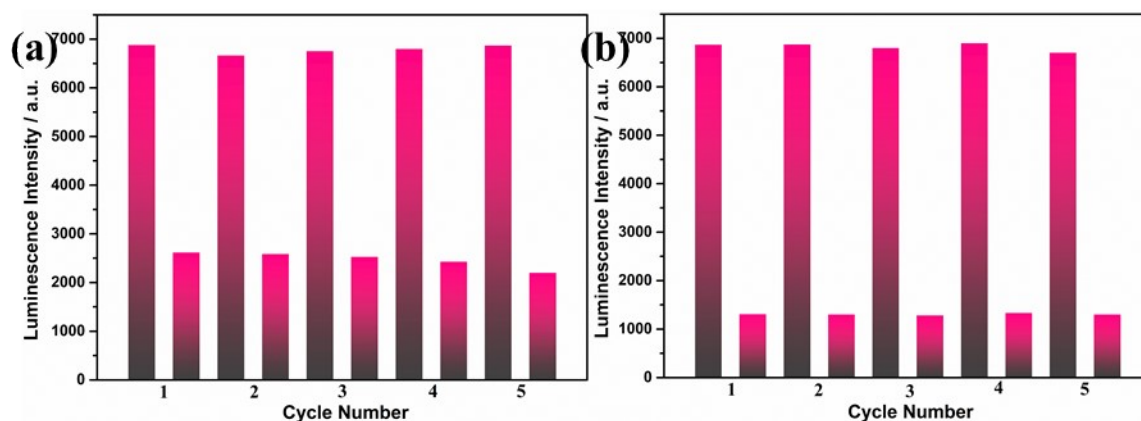
Fig S14. Recycled experimental results: (a) Luminescence intensity at 545 nm of the Eu-MOF in DMF before and after adding PPD (1.5 mM); (b) Luminescence intensity at 545 nm of the Eu-MOF in DMF before and after adding OPD (1.5 mM).

Fig S15. The PXRD spectra of the Ln-MOFs after cycle experiments.

Fig S16. (a) Luminescence decay curve of the Tb-MOF in DMF; (b) Luminescence decay curve of the Tb-MOF in DMF after adding OPD (1.5 mM); (c) Luminescence decay curve of the Tb-MOF in DMF after adding PPD (1.5 mM).
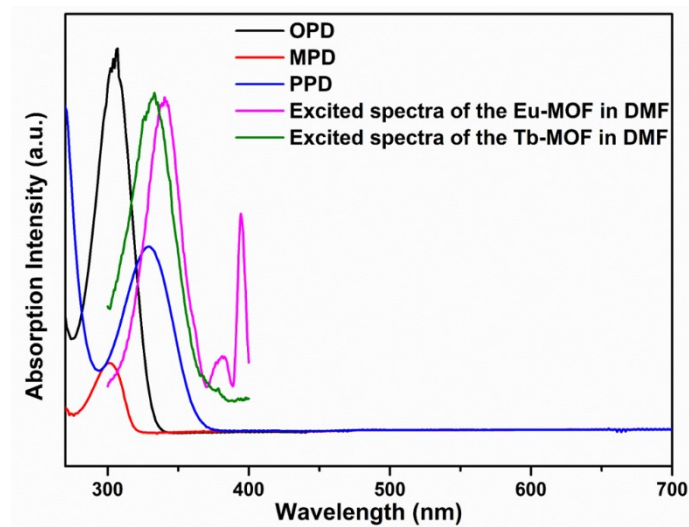
Fig S17. UV-Vis absorption spectra of phenylenediamine in DMF.
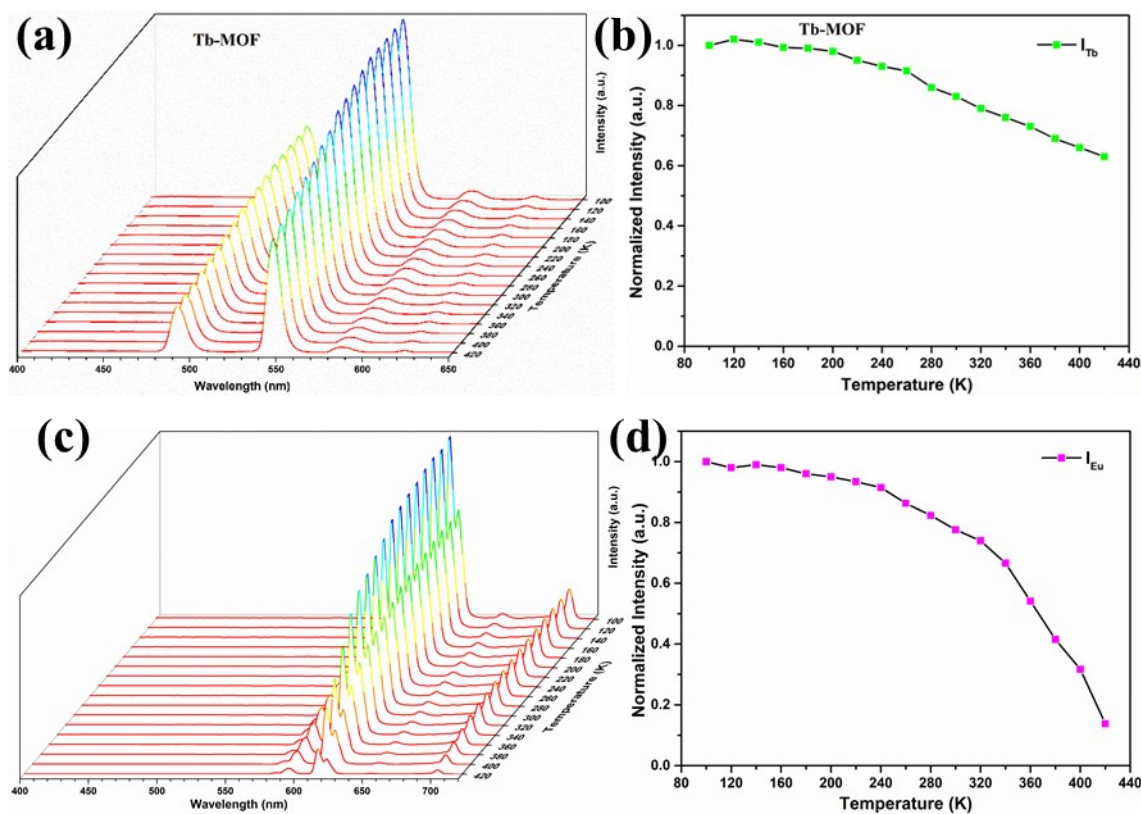
Fig S18. (a) Emission spectra of the Tb-MOF (λ_{em} = 340 nm) in the temperature range from 100 K to 420 K; (b) Corresponding normalized intensity of 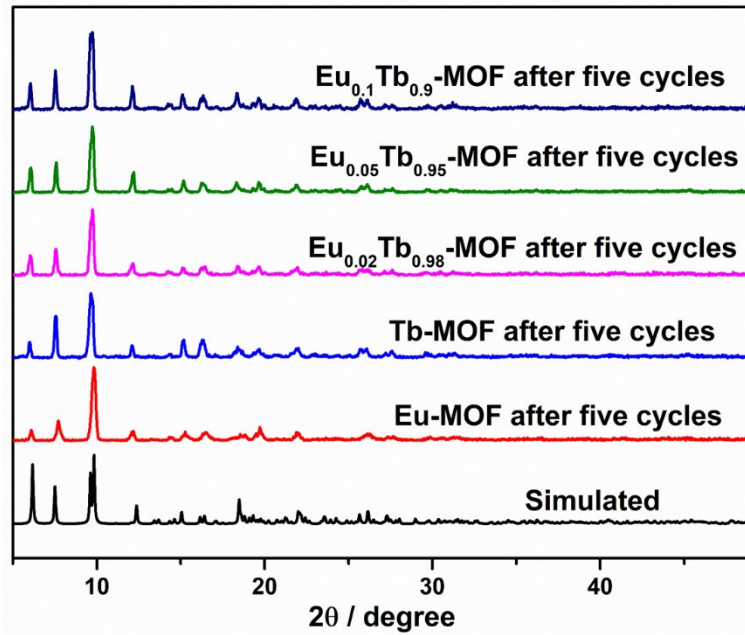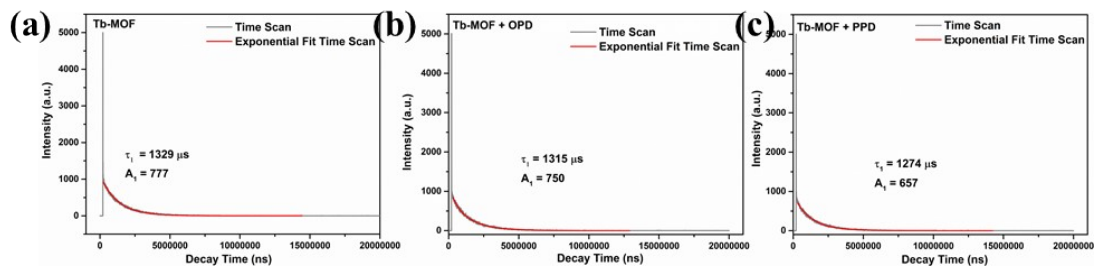the Tb-MOF ($^5D_4 \rightarrow ^7F_5$); (c) Emission spectra of the Eu-MOF (λ_{em} = 340 nm) in the temperature range from 100 K to 420 K; (d) Corresponding normalized intensity of the Eu-MOF ($^5D_0 \rightarrow ^7F_2$).
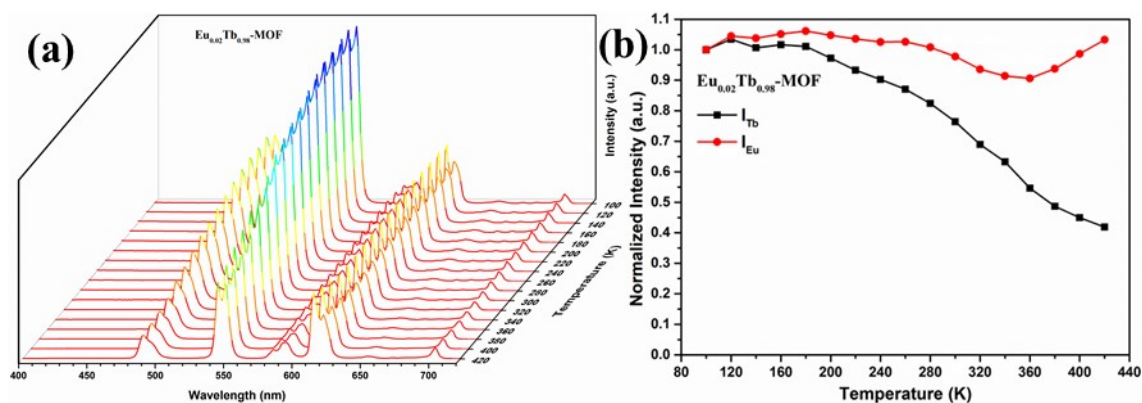
Fig S19. (a) Luminescence spectra of the Eu$_{0.02}$Tb$_{0.98}$-MOF (λ_{ex} = 340 nm) recorded in the temperature range from 100 K to 420 K; (b) Corresponding normalized luminescent intensity of Eu^{3+} ($^5D_0 \rightarrow ^7F_2$) and Tb^{3+} ($^5D_4 \rightarrow ^7F_5$) in the Eu$_{0.02}$Tb$_{0.98}$-MOF.
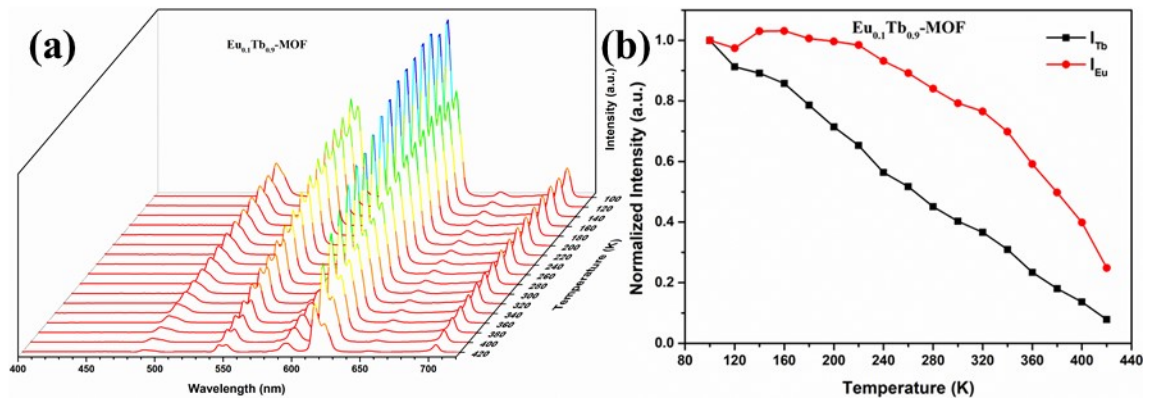
Fig S20. (a) Luminescence spectra of the $Eu_{0.1}Tb_{0.9}$-MOF (λ_{ex} = 340 nm) recorded in the temperature range from 100 K to 420 K; (b) Corresponding normalized luminescent intensity of Eu^{3+} ($^5D_0\rightarrow{}^7F_2$) and Tb^{3+} ($^5D_4\rightarrow{}^7F_5$) in the $Eu_{0.1}Tb_{0.9}$-MOF.
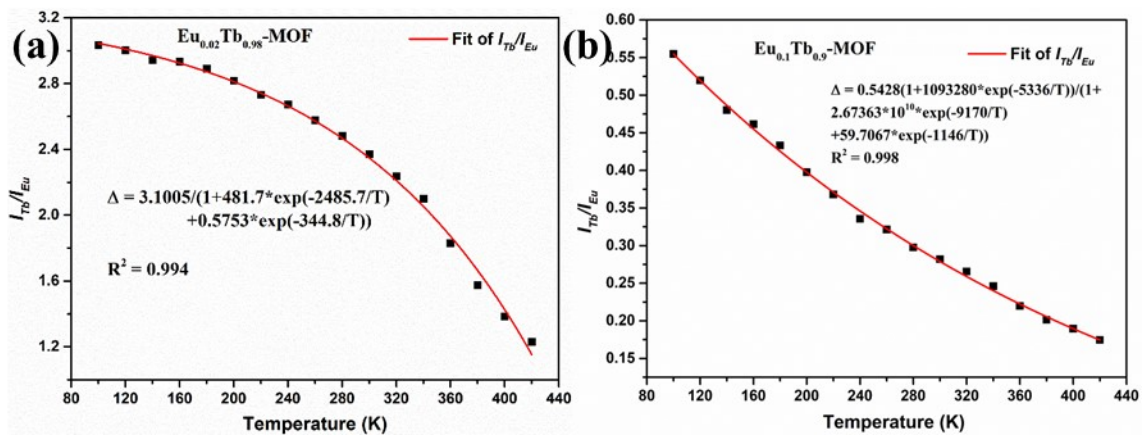

Fig S21. (a) The square symbols represent the measured Δ (I_{Tb}/I_{Eu}) of the $Eu_{0.02}Tb_{0.98}$-MOF and the red curve is the fitted line by Mott-Seitz mode; (b) The square symbols represent the measured Δ (I_{Tb}/I_{Eu}) of the $Eu_{0.1}Tb_{0.9}$-MOF and the red curve is the fitted line by Mott-Seitz mode.
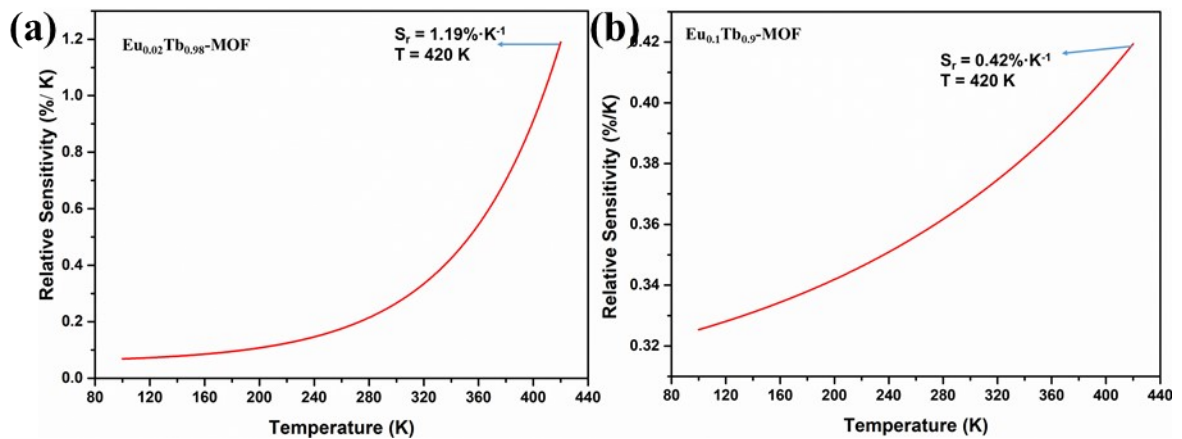
Fig S22. (a) Relative sensitivity (S_r) of the $Eu_{0.02}Tb_{0.98}$-MOF in the temperature from 100 K to 420 K; (b) Relative sensitivity (S_r) of the $Eu_{0.1}Tb_{0.9}$-MOF in the temperature from 100 K to 420 K.
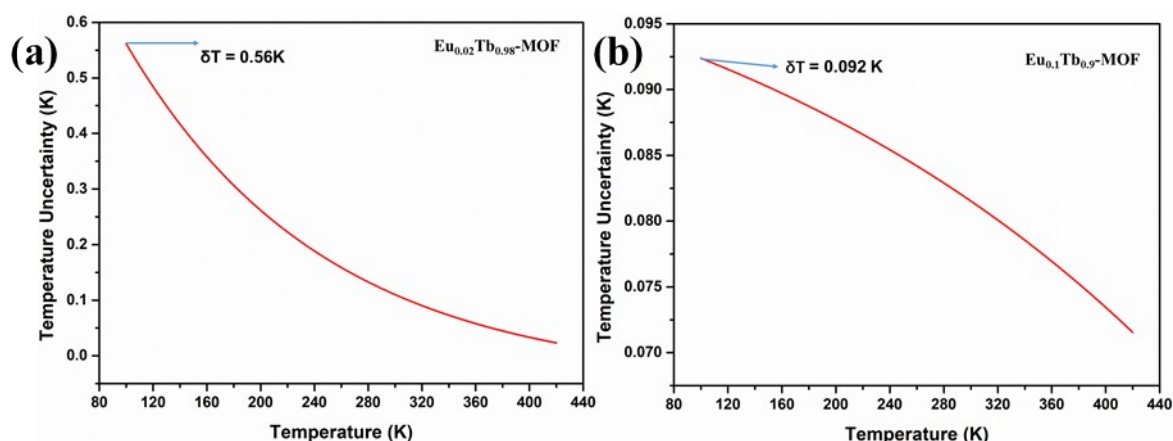
Fig S23. (a) Temperature uncertainty (δT) of the Eu$_{0.02}$Tb$_{0.98}$-MOF in the temperature from 100 K to 420 K; (b) Temperature uncertainty (δT) of the Eu$_{0.1}$Tb$_{0.9}$-MOF in the temperature from 100 K to 420 K.
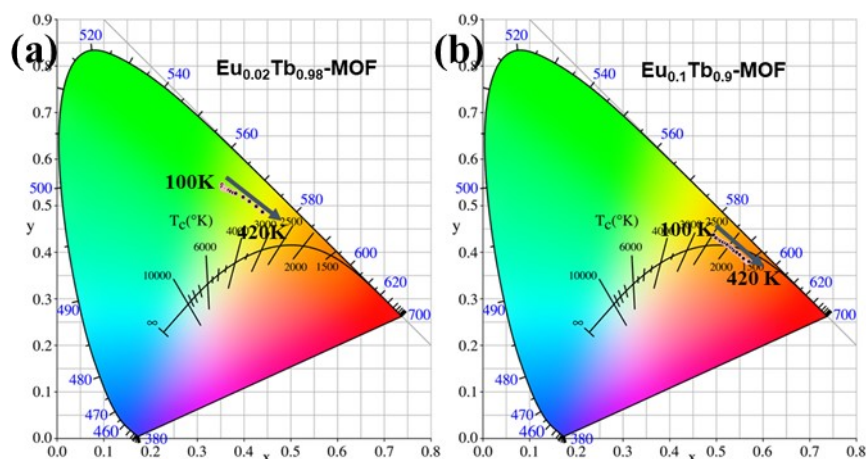
Fig S24. (a) CIE coordinates of the Eu$_{0.02}$Tb$_{0.98}$-MOF when temperature changes from 100 K to 200 K; (b) CIE coordinates of the Eu$_{0.1}$Tb$_{0.9}$-MOF when temperature changes from 100 K to 200 K.
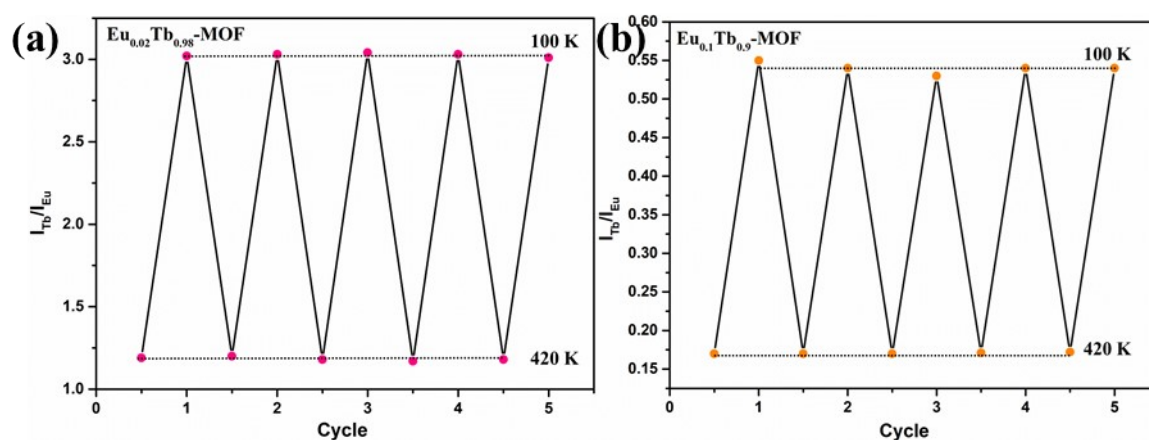
Fig S25. (a) The experimental results of temperature cycles for the Eu$_{0.02}$Tb$_{0.98}$-MOF; (b) The experimental results of temperature cycles for the Eu$_{0.1}$Tb$_{0.9}$-MOF.
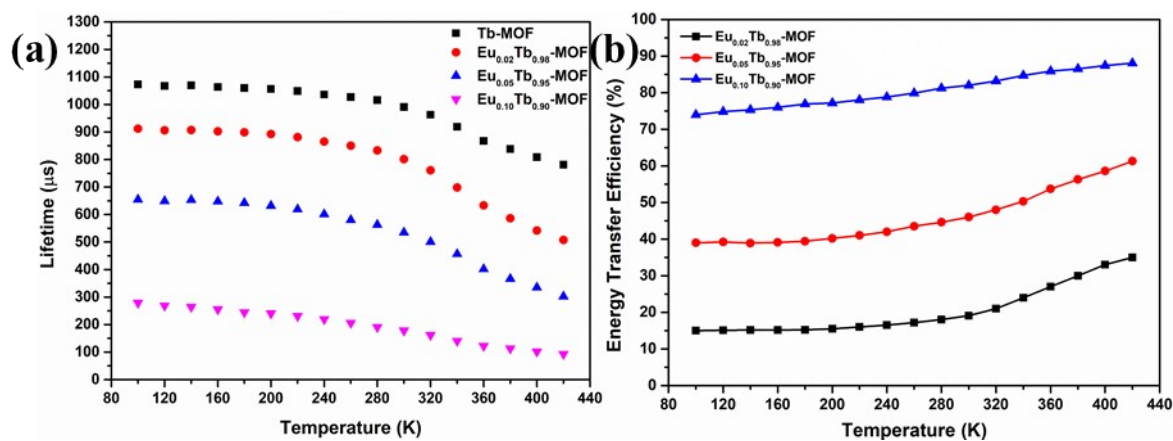
Fig S26. (a) Temperature dependent luminescent times of $^5D_4$ (Tb^{3+}, 545 nm); (b) Energy transfer efficiency between Tb^{3+} ($^5D_4$) and Eu^{3+} ($^5D_1$).
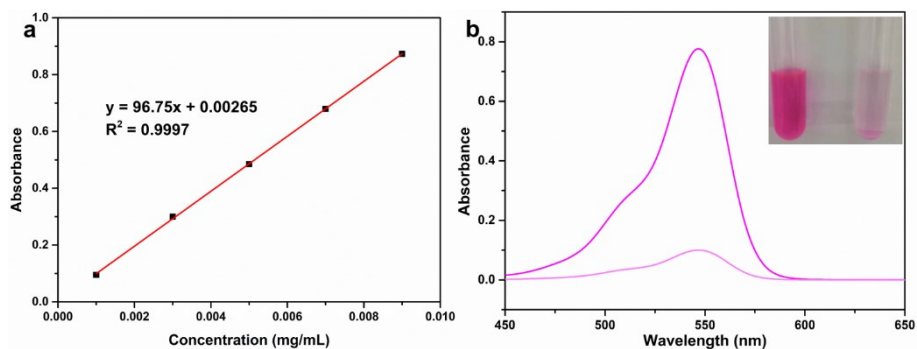
Fig S27. (a) The relationship between the UV-Vis absorbance (monitored the sorption peak at 547 nm) and Rhodamine B concentration in the acetone solution; (b) The UV-Vis spectra of Rhodamine B. Before (deep pink line) and after the addition of the Eu-MOF (light pink line). The insert photograph highlights the sorption effects. Left: before sorption, Right: after sorption.
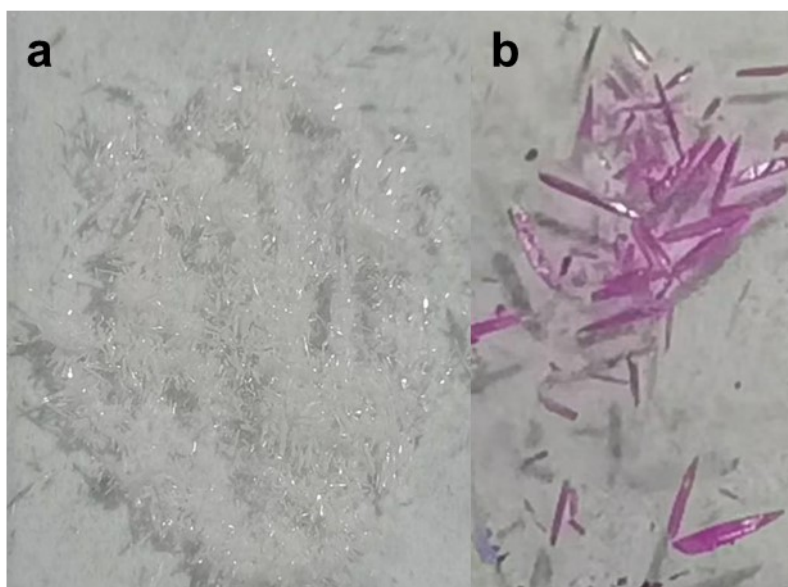
Fig S28. Photo pictures of the crystals of the Eu-MOF: before absorption (a), after sorption of Rhodamine B (b).

Table 1 Crystal data and structure refinement for Eu-MOF

CCDC code	2077564
Empirical formula	$C_{29}H_{33}EuN_4O_{13}$
Formula weight	797.55
Temperature/K	150.00(10)
Crystal system	triclinic
Space group	P-1
a/Å	9.6558(4)
b/Å	11.8403(3)
c/Å	14.3912(9)
α/°	91.242(4)
β/°	90.620(4)
γ/°	91.585(3)
Volume/Å^3	1644.19(13)
Z	2
ρ_{calc}g/cm^3	1.611
μ/mm^{-1}	1.977
F(000)	804.0
Crystal size/mm^3	0.12 × 0.1 × 0.08
Radiation	Mo Kα (λ = 0.71073)
2Θ range for data collection/°	4.22 to 50.048
Index ranges	-11 ≤ h ≤ 11, -13 ≤ k ≤ 14, -17 ≤ l ≤ 16
Reflections collected	11952
Independent reflections	5805 [R_{int} = 0.0430, R_{sigma} = 0.0711]
Data/restraints/parameters	5805/132/472
Goodness-of-fit on F^2	1.072
Final R indexes [I>=2σ (I)]	R_1 = 0.0513, wR_2 = 0.1215
Final R indexes [all data]	R_1 = 0.0587, wR_2 = 0.1281
Largest diff. peak/hole / e Å^{-3}	4.16/-1.12

Table S2. The bond length and bond angles for the Eu-MOF.

Atom	Atom	Length/Å	Atom	Atom	Length/Å
Eu(1)	O(2)	2.443(4)	C(8)	C(9)	1.391(10)
Eu(1)	O(3)	2.507(5)	C(10)	C(11)	1.394(8)
Eu(1)	O(4)	2.481(5)	C(10)	C(15)	1.385(9)
Eu(1)	O(5)	2.427(4)	C(11)	C(12)	1.408(9)

Atom	Atom	Length/Å	Atom	Atom	Length/Å
Eu(1)	O(8)	2.324(5)	C(12)	C(13)	1.359(10)
Eu(1)	O(9)[1]	2.393(4)	C(13)	C(14)	1.390(11)
Eu(1)	O(12)[2]	2.347(4)	C(14)	C(15)	1.392(10)
Eu(1)	O(13)[3]	2.385(4)	C(16)	C(17)	1.507(9)
Eu(1)	C(2)[1]	3.263(6)	C(17)	C(18)	1.405(9)
O(1)	C(1)	1.225(9)	C(17)	C(23)	1.386(9)
O(2)	C(1)	1.271(9)	C(18)	C(19)	1.405(9)
O(8)	C(2)	1.256(8)	C(19)	C(20)	1.393(9)
O(9)	C(2)	1.260(8)	C(20)	C(21)	1.502(9)
O(10)	C(7)	1.231(8)	C(20)	C(22)	1.396(9)
O(11)	C(16)	1.238(8)	C(22)	C(23)	1.400(9)
O(12)	C(21)	1.272(7)	O(6)	C(27)	1.38(3)
O(13)	C(21)	1.254(8)	O(6)	C(27A)	1.15(3)
N(1)	C(7)	1.367(8)	N(3)	C(27)	1.39(2)
N(1)	C(10)	1.430(8)	N(3)	C(28)	1.41(2)
N(2)	C(11)	1.443(8)	N(3)	C(29)	1.418(19)
N(2)	C(16)	1.354(8)	N(3A)	C(27A)	1.40(2)
C(2)	C(3)	1.502(9)	N(3A)	C(29A)	1.40(2)
C(3)	C(4)	1.397(9)	N(3A)	C(28A)	1.414(18)
C(3)	C(9)	1.385(9)	O(7)	C(24)	1.279(11)
C(4)	C(5)	1.378(9)	N(4)	C(24)	1.306(11)
C(5)	C(6)	1.402(9)	N(4)	C(25)	1.430(13)
C(6)	C(7)	1.488(9)	N(4)	C(26)	1.440(12)
C(6)	C(8)	1.399(9)			

[1]1-X,1-Y,1-Z; [2]+X,1+Y,+Z; [3]2-X,-Y,1-Z

Atom	Atom	Atom	Angle/°	Atom	Atom	Atom	Angle/°
O(2)	Eu(1)	O(3)	73.77(16)	C(9)	C(3)	C(2)	120.3(6)
O(2)	Eu(1)	O(4)	124.84(16)	C(9)	C(3)	C(4)	119.3(6)
O(2)	Eu(1)	C(2)[1]	139.98(15)	C(5)	C(4)	C(3)	119.9(6)
O(3)	Eu(1)	C(2)[1]	66.74(16)	C(4)	C(5)	C(6)	121.3(6)
O(4)	Eu(1)	O(3)	132.56(17)	C(5)	C(6)	C(7)	117.9(6)
O(4)	Eu(1)	C(2)[1]	88.25(16)	C(8)	C(6)	C(5)	118.4(6)
O(5)	Eu(1)	O(2)	139.06(17)	C(8)	C(6)	C(7)	123.7(6)
O(5)	Eu(1)	O(3)	124.30(16)	O(10)	C(7)	N(1)	123.1(6)
O(5)	Eu(1)	O(4)	72.99(16)	O(10)	C(7)	C(6)	121.2(6)
O(5)	Eu(1)	C(2)[1]	66.22(17)	N(1)	C(7)	C(6)	115.6(5)
O(8)	Eu(1)	O(2)	78.43(16)	C(9)	C(8)	C(6)	120.0(6)

Atom	Atom	Atom	Angle/°	Atom	Atom	Atom	Angle/°
O(8)	Eu(1)	O(3)	77.65(16)	C(3)	C(9)	C(8)	121.0(6)
O(8)	Eu(1)	O(4)	143.27(16)	C(11)	C(10)	N(1)	122.8(6)
O(8)	Eu(1)	O(5)¹	71.79(16)	C(15)	C(10)	N(1)	118.3(5)
O(8)	Eu(1)	O(9)¹	105.75(16)	C(15)	C(10)	C(11)	118.8(6)
O(8)	Eu(1)	O(12)²	86.22(16)	C(10)	C(11)	N(2)	123.8(6)
O(8)	Eu(1)	O(13)³	143.79(16)	C(10)	C(11)	C(12)	119.2(6)
O(8)	Eu(1)	C(2)¹	86.97(16)	C(12)	C(11)	N(2)	117.0(5)
O(9)¹	Eu(1)	O(2)	143.54(16)	C(13)	C(12)	C(11)	121.1(7)
O(9)¹	Eu(1)	O(3)	71.97(17)	C(12)	C(13)	C(14)	120.3(7)
O(9)¹	Eu(1)	O(4)	73.18(16)	C(13)	C(14)	C(15)	119.0(6)
O(9)¹	Eu(1)	O(5)	73.14(18)	C(10)	C(15)	C(14)	121.5(6)
O(9)¹	Eu(1)	C(2)¹	18.78(16)	O(11)	C(16)	N(2)	123.6(6)
O(12)²	Eu(1)	O(2)	71.79(15)	O(11)	C(16)	C(17)	121.0(6)
O(12)²	Eu(1)	O(3)	144.22(16)	N(2)	C(16)	C(17)	115.3(5)
O(12)²	Eu(1)	O(4)	77.04(16)	C(18)	C(17)	C(16)	117.1(6)
O(12)²	Eu(1)	O(5)	78.72(16)	C(23)	C(17)	C(16)	123.8(6)
O(12)²	Eu(1)	O(9)¹	143.71(16)	C(23)	C(17)	C(18)	119.0(6)
O(12)²	Eu(1)	O(13)³	105.49(15)	C(17)	C(18)	C(19)	120.4(6)
O(12)²	Eu(1)	C(2)¹	144.66(15)	C(20)	C(19)	C(18)	120.2(6)
O(13)³	Eu(1)	O(2)	73.31(17)	C(19)	C(20)	C(21)	121.4(5)
O(13)³	Eu(1)	O(3)	73.09(15)	C(19)	C(20)	C(22)	119.1(6)
O(13)³	Eu(1)	O(4)	72.80(16)	C(22)	C(20)	C(21)	119.5(6)
O(13)³	Eu(1)	O(5)	143.48(17)	O(12)	C(21)	C(20)	118.7(6)
O(13)³	Eu(1)	O(9)¹	85.08(17)	O(13)	C(21)	O(12)	123.6(6)
O(13)³	Eu(1)	C(2)¹	100.34(16)	O(13)	C(21)	C(20)	117.6(5)
C(1)	O(2)	Eu(1)	137.4(5)	C(20)	C(22)	C(23)	120.8(6)
C(2)	O(8)	Eu(1)	170.9(4)	C(17)	C(23)	C(22)	120.5(6)
C(2)	O(9)	Eu(1)¹	123.5(4)	C(27)	N(3)	C(28)	132.3(19)
C(21)	O(12)	Eu(1)⁴	164.2(4)	C(27)	N(3)	C(29)	108.7(17)
C(21)	O(13)	Eu(1)³	127.9(4)	C(28)	N(3)	C(29)	117.8(14)
C(7)	N(1)	C(10)	122.5(5)	O(6)	C(27)	N(3)	106(2)
C(16)	N(2)	C(11)	123.6(5)	C(27A)	N(3A)	C(29A)	133.3(18)
O(1)	C(1)	O(2)	128.0(8)	C(27A)	N(3A)	C(28A)	107.2(17)
O(8)	C(2)	Eu(1)¹	86.3(4)	C(29A)	N(3A)	C(28A)	118.8(15)
O(8)	C(2)	O(9)	123.8(6)	O(6)	C(27A)	N(3A)	151(3)
O(8)	C(2)	C(3)	119.3(6)	C(24)	N(4)	C(25)	120.6(8)
O(9)	C(2)	Eu(1)¹	37.7(3)	C(24)	N(4)	C(26)	123.4(9)
O(9)	C(2)	C(3)	116.9(6)	C(25)	N(4)	C(26)	116.0(9)

Atom	Atom	Atom	Angle/°	Atom	Atom	Atom	Angle/°
C(3)	C(2)	Eu(1)[1]	154.1(4)	O(7)	C(24)	N(4)	124.5(9)
C(4)	C(3)	C(2)	120.4(6)				

[1]1-X,1-Y,1-Z; [2]+X,1+Y,+Z; [3]2-X,-Y,1-Z; [4]+X,-1+Y,+Z

Table S3. The molar ratio of Eu and Tb in the Eu_xTb_{1-x}-MOF calculated by ICP analysis.

Sample	The molar ratio of Eu and Tb
$Eu_{0.02}Tb_{0.98}$-MOF	0.0223:0.9777
$Eu_{0.05}Tb_{0.95}$-MOF	0.0598:0.9402
$Eu_{0.1}Tb_{0.9}$-MOF	0.1125:0.8875

Table S4. Calculated excited states and HOMO-LUMO energy levels of the H_2L

Basis set	6-31G (d)			
Excited state	Triplet (eV)			Singlet (eV)
	T_1	T_2	T_3	3.6387
H_2L	2.8848 (429.78 nm) (23268 cm^{-1})	3.2493	3.3336	(340.74 nm) (29348 cm^{-1})

Table S5. Comparing the K_{SV} of the luminescent MOF sensors detecting OPD and PPD

Luminescent MOF	samples	K_{SV} (M^{-1})	Ref
Tb-MOF	OPD	1451	This work
	PPD	4726	
Eu-MOF	OPD	1034	
	PPD	2750	
Bi-MOF	OPD	54000	[1]
Cu-MOF	OPD	608.6	[2]

Table S6. Comparing the performance of the luminescent MOF thermometers in terms of temperature range, maximum relative sensitivity (S_r) and corresponding temperature (T_m)

Luminescent MOF	Range (K)	S_r (% K^{-1})	T (K)	Ref

$Eu_{0.02}Tb_{0.98}$-MOF	100~420 K	1.19	420	This work
$Eu_{0.05}Tb_{0.95}$-MOF		1.01	420	
$Eu_{0.1}Tb_{0.9}$-MOF		0.42	420	
$Tb_{0.99}Eu_{0.01}(BDC)_{1.5}$-$(H_2O)_2$	290~320 K	0.31	318	3
$Tb_{0.80}Eu_{0.20}BPDA$	298~318 K	1.19	313	4
$Eu_{0.05}Tb_{0.95}BDC$-OH	313~513 K	1.55	440	5
$Eu_{0.05}Tb_{0.95}$-2Me	313~473 K	1.76	353	6

Notes and references

1. R. Huo, Y. Sun, Y. H. Xing, F. Y. Bai and L. X. Sun, *J Mol Struct*, 2021, **1228**.

2. Q. L. Guan, Y. Sun, R. Huo, Y. Xin, F. Y. Bai, Y. H. Xing and L. X. Sun, *Inorg Chem*, 2021, **60**, 2829-2838.

3. A. Cadiau, C. D. S. Brites, P. M. F. J. Costa, R. A. S. Ferreira, J. Rocha and L. D. Carlos, *Acs Nano*, 2013, **7**, 7213-7218.

4. D. Zhao, X. T. Rao, J. C. Yu, Y. J. Cui, Y. Yang and G. D. Qian, *Inorg Chem*, 2015, **54**, 11193-11199.

5. X. S. Lian, D. Zhao, Y. J. Cui, Y. Yang and G. D. Qian, *Chem Commun*, 2015, **51**, 17676-17679.

6. J. W. Liu, X. Han, Y. T. Lu, S. Wang, D. Zhao and C. X. Li, *Inorg Chem*, 2021, **60**, 4133-4143.